Lasers in Medical Science (2020) 35:585–597
https://doi.org/10.1007/s10103-019-02852-y

ORIGINAL ARTICLE

Photobiomodulation therapy can change actin filaments of 3T3 mouse fibroblast

Ana Carolina de Magalhães [1,2] · Zwinglio Guimarães-Filho [1] · Elisabeth Mateus Yoshimura [1] · Lothar Lilge [3]

Received: 30 April 2019 / Accepted: 23 July 2019 / Published online: 13 August 2019

Abstract

The purpose of this study was to investigate the effects that photobiomodulation therapy might produce in cells, in particular, related to their structure. Thus, this paper presents the results of morphological changes in fibroblasts following low-intensity light illumination. Mouse fibroblasts were grown on glass coverslips on either 4 kPa or 16 kPa gels, to mimic normal tissue conditions. Cells were photo-irradiated with laser light at either 625 nm or 808 nm (total energies ranging from 34 to 47 J). Cells were fixed at 5 min, 1 h, or 24 h after photo-irradiation, stained for both actin filaments and the cell nucleus, and imaged by confocal microscopy. A non-light exposed group was also imaged. A detailed analysis of the images demonstrated that the total polymerized actin and number of actin filaments decrease, while the nucleus area increases in treated cells shortly after photo-irradiation, regardless of substrate and wavelength. This experiment indicated that photobiomodulation therapy could change the morphological properties of cells and affect their cytoskeleton. Further investigations are required to determine the specific mechanisms involved and how this phenomenon is related to the photobiomodulation therapy mechanisms of action.

Keywords Photobiomodulation therapy · Fibroblasts · Actin filaments · Low-level light therapy

Introduction

The interest, use, and research of photobiomodulation therapy (PBMT) is growing in health care due to its well-established wound healing and analgesic, anti-inflammatory, and anti-oedematous effects [1]. PBMT is non-invasive and practically does not have demonstrated side effects. The PBMT action is not associated with thermal effects, but due to other photophysical and photochemical responses at the cellular level. The most reported PBMT mechanism of action is the absorption of photons by cytochrome C oxidase, a component of the respiratory chain, in the mitochondria. This appears to result in a modulation of the ATP synthesis, the release of signalling molecules including reactive oxygen species and nitric oxides resulting in the stimulation of cell proliferation and wound healing. Although light absorption by cytochrome C oxidase is well established, there are references to other possible mechanisms and some effects cannot be explained by the cytochrome absorption. Thus, all mechanisms of PBMT are not well understood [2–5].

Fibroblasts are the most abundant cell type in mammalians and are found in most organs. In adult individuals, fibroblast's primary function is in the constant tissue remodelling and to help in the wound healing process, particularly in the skin. Furthermore, they are responsible for the synthesis of extracellular matrix in connective tissues [6, 7]. Many studies have shown that PBMT modulates, mainly stimulate, the cell proliferation of fibroblasts [8].

During wound repair, the fibroblast needs to move over and through the wound, for which the cytoskeleton, a filament network composed of small fibres present in the cytoplasm, is responsible. The cytoskeleton is also responsible for maintaining the cell structure, transport of organelles, and their location in the cytoplasm, among other functions. The actin filaments represent one type of cytoskeleton and are more abundant near the plasmatic membrane. Their roles are related to cell migration, division and structure, and processes associated with wounding healing. The actin remodelling is

✉ Ana Carolina de Magalhães
anamagalhaes@usp.br

[1] Institute of Physics, University of Sao Paulo, São Paulo, Brazil

[2] Insper, São Paulo, Brazil

[3] Department of Medical Biophysics, University of Toronto, Toronto, Canada

indispensable for cell migration. Furthermore, the integrity of the cytoskeleton and the cell membrane is essential for cell viability and proliferation [9]. In cell culture, the substrate rigidity might influence remodelling and dynamics of the cytoskeleton [10, 11].

The cytoskeleton is highly integrated with the cell nucleus. There are direct attachments of the cytoskeleton and the nuclear membrane, mainly connection between the actin filaments and the nucleoskeleton (a network responsible for the nucleus structure, and equivalent to the cytoskeleton, inside the nucleus) [11]. During the cell migration, the nucleus movement is crucial, as it is the largest organelle and its compression is difficult. The cytoskeleton mediates this migration, in particular, a network composed of actin and myosin (a molecular motor) both involved in cell contraction [10].

There are some reports of effects of the PBMT in the cytoskeleton. Chow and colleagues [12] showed that transient conformational changes in the axon microtubules are responsible for modulating nerve impulse transmission and inhibition of pain. Also, Ricci and colleagues [13] showed that the PBMT can reestabilish cell homeostasis, with remodelling of the actin filaments of cells that were restricted of growing factors, thus the filaments showed organization similar to healthy cells. Furthermore, Houreld and colleagues [14] showed that the PBMT can change gene expression of healthy cells, including genes related to cytoskeleton with functions such as mobility, cell structure and integrity, and cytoskeleton reorganization. However, they did not determined the specific effects of these expression changes, in particular if the cytoskeleton function was modified. However, none of these studies were performed in fibroblasts; in fact, few papers showed that illumination of fibroblasts with visible and near-infrared (NIR) light, in particular with laser light, can affect the cytoskeleton. The mechanisms, however, are still not fully understood [15, 16].

The objective of this study was to investigate further the effects of PBMT mediated by red and NIR light on changes in the morphological characteristics of fibroblasts via modifications of its cytoskeleton.

Materials and methods

Experimental setup

Cell culture

Cells of mouse fibroblast, lineage 3T3, were cultivated with DMEM media supplemented with penicillin and streptomycin, L-glutamine, sodium pyruvate, and 10% fetal bovine serum (FBS), and kept at 37 °C, 10% carbon dioxide. For the experiment, the cells were grown on glass coverslips covered with a polyacrylamide gel, whose preparation protocol was adapted from Fischer and colleagues [17] and tested previously [18]. Two different gel stiffness were used: 4 kPa and 16 kPa, to mimic the normal conditions cells in soft tissues such as brain and stronger tissue including skin wounds [19]. Cells were kept in a light-protected incubator prior to the experiments and after PBM treatment until experimental readout. For experimental preparation, the environmental light exposure was minimized < 10 mW cm^{-2}.

Photobiomodulation treatment

A 96-laser diode array module (Theralase Inc., Toronto, ON, Canada) was used for the fibroblast PBM treatment, generating a flat illumination field beyond a light diffusing layer. Light parameters are shown in Table 1. The time interval between the plating process and the PBM treatment was either 6 h or 24 h depending on the incubation time between the PBM treatment and the fixing. This incubation time was chosen to control fibroblast proliferation and to keep fibroblasts in a monolayer. After the treatment, cells were incubated until they were fixed and stained.

Fluorescent staining

The cells were fixed with methanol-free 4% formaldehyde solution at three different time intervals after PBM treatment: 5 min, 1 h, or 24 h. The fibroblast permeabilization was performed with 0.1% Triton X-100 solution (Sigma-Aldrich, Oakville, Ontario, Canada). Fibroblasts were stained with two different fluorescent probes: the Alexa Fluor 488 Phalloidin (AF488) for actin filaments, and 4′,6-diamidino-2-phenylindole dihydrochloride (DAPI) for the cell nucleus (both from Thermo Fisher Scientific, Markham, Ontario, Canada). The coverslips were mounted on glass slides using ProLong Gold antifade reagent (Thermo Fisher Scientific). The glass slides were kept at room temperature for 24 to 72 h to dry and then stored in the refrigerator.

Confocal microscopy

For cell morphology image acquisition, an inverted confocal microscope (LSM700 Zeiss, Toronto, Canada) was used equipped with a 40 ×, 1.4 NA oil immersion objective. Proprietary software (LSM Zen 2012) was used for image acquisition. Solid-state lasers excited the samples with either 405 nm (for DAPI) or 488 nm (for AF488). Emission intensities were collected in separate channels, called DAPI for the former related to the cell nuclei and AF488 for the actin-associated signal. Each pixel signal was averaged over two repeat samplings.

The images are in 8-bit format. For each field of view, data acquisitions were carried out in different depths of the sample. Thus, each dataset is comprised of a stack encompassing

Table 1 Light source parameters used in the photobiomodulation treatment. The area considered to calculate the power and energy was the coverslip area (1.13 cm^2), as the module has multiple diode lasers the photometric values are not homogenous across the samples but are represented by a mean value and a uncertainty, which is the number in parentheses after the value

Wavelength [nm]	625 (red)	808 (IR)
Irradiance [mW cm^{-2}]	115 (8)	125 (8)
Radiant power per well [mW]	130 (9)	141 (9)
PBM treatment time [s]	300	300
Radiant exposure [J cm^{-2}]	35 (3)	38 (3)
Radiant energy per well [J]	39 (3)	42 (3)

multiple optical sections. Each optical section corresponds to an image acquired in a different depth within the field of view.

Replication and pairing

For each experiment, there were three externally controlled experimental parameters:

- Wavelength—the cells were PBM-treated with either red (625 nm) or infrared (808 nm) light;
- Gel stiffness—the cells were grown in gels with either 4 kPa or 16 kPa;
- Time post-PBM treatment—the cells were incubated for 5 min, 1 h, or 24 h after the PBM treatment prior to fixation.

Each combination of the experimental parameters was numbered and considered an independent experiment, as shown in Table 2. All experimental conditions were repeated at least twice for each experiment. For all experiments, the samples were divided into two sub-groups: a control and a PBM-treated one.

Analysis

Image analysis

The images were analysed with Fiji (a distribution of the NIH software ImageJ) [20] utilizing MATLAB software environment [21], to automatize image evaluation. Four variables from each image were considered: cell area, nuclear area, number of filaments, and total actin. The number of replications, for each analysed variable, is the same as the number of replications of the experiments performed, as indicated in Table 2.

For the *cell area* (*CAr*), all images in a stack were projected into one image, the cell was delineated, and its area quantified. We estimated the cell area as the portion of the image where

Table 2 Description of the experimental parameters of each experiment performed. The first column is related to the wavelength used for the photobiomodulation (PBM) treatment, according to Table 1. The last column refers to the gel stiffness of the substrate where the cells were grown. The lines represent the experiments with those parameters, for example, cells from experiments 1 to 3 were grown in 4 kPa gels and PBM-treated with red light, while cells from experiments 4 to 6 were grown in 16 kPa gels and were also PBM-treated with red light. The time lack, between the PBM treatment and the fixation process, is indicated. At last, the number in parentheses shows the number of replications performed for each experiment, including all repetitions and/or sections on the confocal microscope, for each analysed variable

PBM treatment	Experiments (number of measurements done) Incubation time, between PBM treatment and fixing			Gel stiffness
Red	Experiment 1 (3×)	Experiment 2 (5×)	Experiment 3 (2×)	4 kPa
	5 min	1 h	24 h	
	Experiment 4 (2×)	Experiment 5 (2×)	Experiment 6 (2×)	16 kPa
	5 min	1 h	24 h	
IR	Experiment 7 (2×)	Experiment 8 (2×)	Experiment 9 (3×)	4 kPa
	5 min	1 h	24 h	
	Experiment 10 (2×)	Experiment 11 (2×)	Experiment 12 (2×)	16 kPa
	5 min	1 h	24 h	

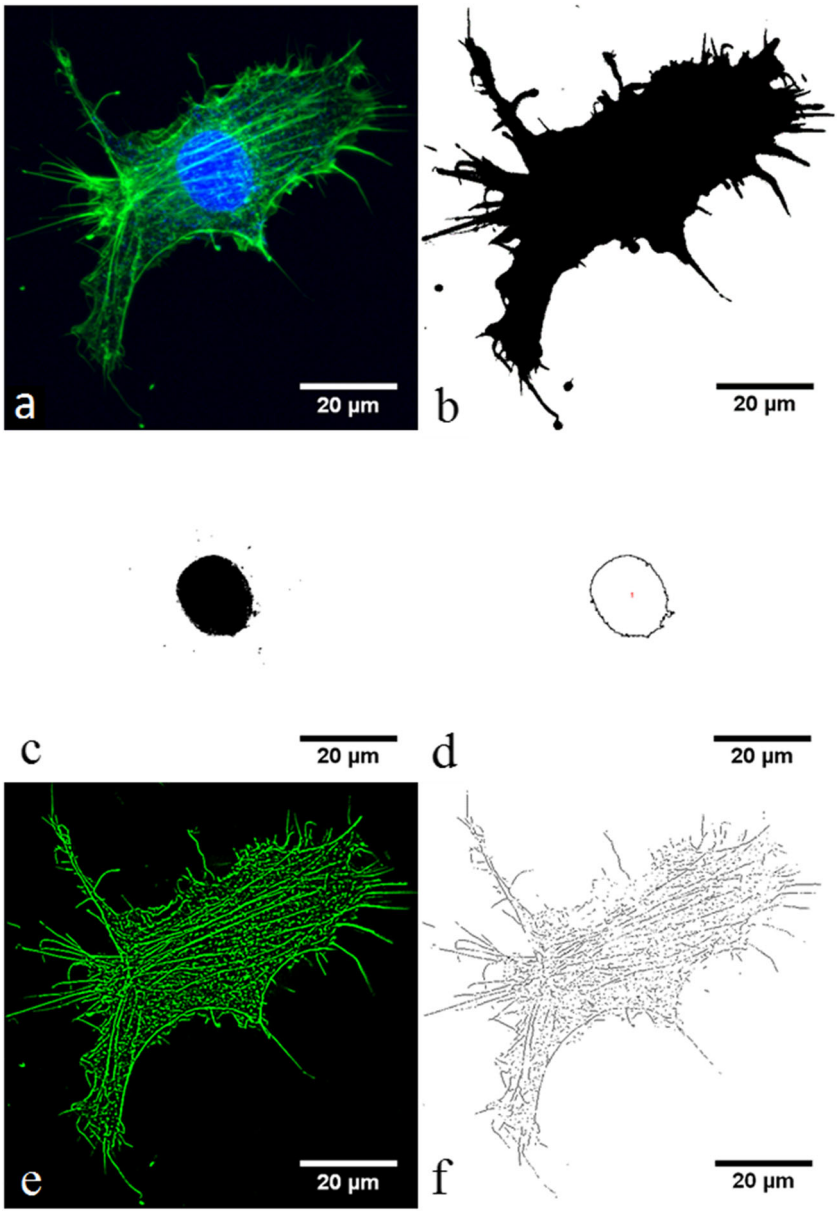

Fig. 1 Examples of the image processing sequence for analysis. (**a**) 2D projection of the 3D image stack, yielding the maximum intensities for both the DAPI fluorescence (blue—DAPI channel) and actin filaments fluorescence (green—AF488 channel). (**b**) Determination of the cross-sectional cell area, by converting the AF488 channel into a 2-bit, black and white image, black representing the cell area. (**c**) Nuclear area proceeded similarly using the DAPI channel image. (**d**) Delimitation of the black area identified for the nuclear area, it permitted counting the number of cells in the image. (**e**) The actin filaments associated fluorescence was enhanced. (**f**) Determination of the primary actin structures to count the number of filaments in the image

actin filament staining was visible [22]. Therefore, the AF488 channel was used to determine this variable (see Fig. 1 a and b).

The *nuclear area* (*NAr*) was determined using the DAPI channel. The region of the image containing the nucleus was identified, and its area quantified (see Fig. 1 c and d).

The *number of filaments* (*NuF*) was evaluated using the AF488 channel. The filaments were enhanced, as shown in Fig. 1e, and the primary structure of the filaments was determined, as shown in Fig. 1f [23, 24]. After that, the number of filaments in the image was calculated as the sum of all branches, regardless of the branch size.

The *total amount of actin* (*ToA*) was estimated based on the intensity, using the AF488 channel. The fluorescence intensities of all stack images were summed, excluding background pixels.

Data analysis

The raw data was analysed to verify the number of cells in the images and the distribution of cell density per image. A detailed description of these analysis and the results are presented in the Appendix (Raw data analysis subsection), Figs. 6 and 7. A linear function $Y(N) = aN$ (where Y is the analysed variable *NAr*, *CAr*, *NuF*, or *ToA*, N is the number of cells in the image, and a is the slope) would be adequate only for images with low cell densities. However, in order to adjust for the deviation from linearity at high cell densities, a fit required a small quadratic term as shown in Eq. 1, where γ was determined from the global relation between Y and N for all data.

$$Y(N) = aN(1-\gamma N) \quad (1)$$

The uncertainty, σ_N, for each $Y(N)$ variable (*NAr*, *CAr*, *NuF*, or *ToA*) was determined as a function of the image's cell density. The full description can be found in the Appendix (Raw data analysis subsection).

Due to the natural variation of the cell culture used for each measurement, the cell properties are slightly different between experiments, and therefore, all the analyses were performed considering the relationship between the PBM-treated group concerning the corresponding control group (paired method). However, to simplify the representation of the data in the fittings, the graphs show the global average value of the variables concerning the number of cells with the error bar representing the standard deviation of the mean value (standard error of the mean).

The slopes of the PBM-treated (a_{PT}) and control (a_{Ct}) groups of each measurement, fitted using Eq. 1, were compared through their relative differences (β), as shown in Eqs. 2 and 3. Thus, the difference of the two sample populations is emphasized. Hence, if the β coefficient is different from zero, it means that (a_{PT}) the PBM-treated group slopes are different from (a_{Ct}) the control group slopes.

$$a_{PT} = (1 + \beta)\, a_{Ct} \tag{2}$$

$$\beta = \frac{a_{PT} - a_{Ct}}{a_{Ct}} \tag{3}$$

The first analysis was to compare the PBM-treated samples with the control groups globally, regardless of the experimental parameters (wavelength, gel stiffness, and time post-PBM treatment) used in the experiment. Therefore, in the first fit, the β coefficient was considered the same for all experiments in order to see the average effect produced by the PBM treatment.

In the second level of analysis, the effects of the experimental parameters were analysed. For that, the separation of data was performed according to the parameter value (for instance, the PBM-treated and control samples were separated by wavelength) and the same analysis described above was executed. Thus, there are two β values, one for each wavelength (β_{red} and β_{IR}). The same was completed for the experimental parameters gel stiffness (resulting in β_{4kPa} and β_{16kPa}), and time post-PBM treatment (resulting in β_{5min}, β_{1h}, and β_{24h}). By this approach, the influence of each investigated experimental condition was analysed separately.

At last, all experimental parameters were considered all together and analysed in a single fitting.

Statistical analysis

The least square method was used to fit data according to the considered models and the χ^2 the goodness of fit was used to estimate the uncertainties. The *Z* test was used to compare the

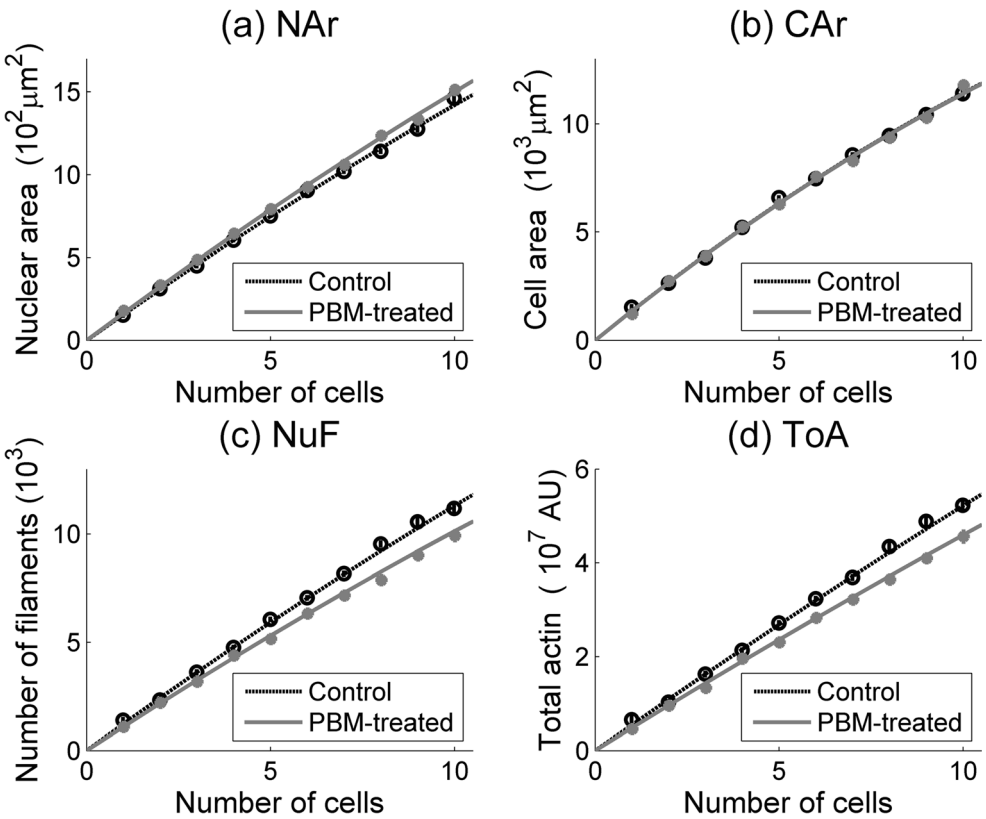

Fig. 2 Graphs for each analysed variable, nuclear area *NAr* (**a**), cell area *CAr* (**b**), number of filaments *NuF* (**c**), and total actin *ToA* (**d**), with the separation only between control (black symbols) and photobiomodulation-treated (grey symbols) groups. The total number of images was 1693 (837 for the control group and 856 for the photobiomodulation-treated group). The error bars indicate the standard error of the mean (SEM); however, for most of the points, the error bars are smaller than the symbols

Table 3 Coefficient β for all the analysed variables, nuclear area *NAr*, cell area *CAr*, number of filaments *NuF*, and total actin *ToA*. Two asterisk symbols indicate that the coefficients are different from zero, according to the *Z* test and $p < 0.01$. The number in parentheses is the uncertainty of the coefficient in the last(s) decimal(s)

Coefficient	*NAr*	*CAr*	*NuF*	*ToA*
β	+ 0.051 (8)**	− 0.005 (9)	− 0.106 (9)**	− 0.123 (11)**

fitted coefficients between groups and with zero. The *Z* test is equivalent to the *t* test in this case because the uncertainties were estimated with a large number of degrees of freedom (~ 1660). The compatibility was checked according to the *p*-values, and cases with $p < 0.01$ were considered incompatible. Cases with $p < 0.05$ were also indicated. The *p* values for all the 84 statistical tests performed in this work are in the Appendix (*p* values of the statistical tests subsection).

Results

Global analysis

Figure 2 shows the average value of each variable for the control and PBM-treated groups, as a function of the cell number per image (*N*). Figure 2 c and d show that the values of the *NuF*, and the *ToA*, are smaller for the PBM-treated cells than for control cells. Furthermore, the difference between the control and PBM-treated groups increases with the number of cells, consistent with the expectation of an average alteration per cell. The same behaviour, but in the opposite direction, is observed for the *NAr* (Fig. 2a), whereas no difference is noted in the *CAr* (Fig. 2b).

Table 3 shows the results for the β coefficient, defined in Eqs. 2 and 3, for all analysed variables. Except for the *CAr*, all β coefficients are significantly different from zero. On average, the *NAr* is around 5% higher when comparing the PBM-treated group with the control group. On the other hand, the *NuF* and the *ToA* are respectively around 11% and 12% lower for the PBM-treated group, when compared with the control group. The fact that for the PBM groups the *NAr*, *NuF*, and *ToA*, are different from the control groups, independent of the confounding factors of wavelength, gel stiffness, and time post-PBM, indicates photon-mediated changes to the cytoskeleton. After demonstrating a global influence of the PBM treatment, we evaluated each of the experimental parameters separately to their influence on these observations.

Influence of the experimental parameters

Firstly, wavelength, gel stiffness, and time post-PBM treatment were considered, one at a time, followed by a final fitting with all parameters considered at the same time to isolate the contribution of each on the cytoskeletal changes.

Influence of each parameter individually

The results for the separation according to the wavelength used in the PBM treatment are shown in Fig. 3 and Table 4. Note that no significant difference between β for the red and IR wavelengths is observed, despite the β coefficients being

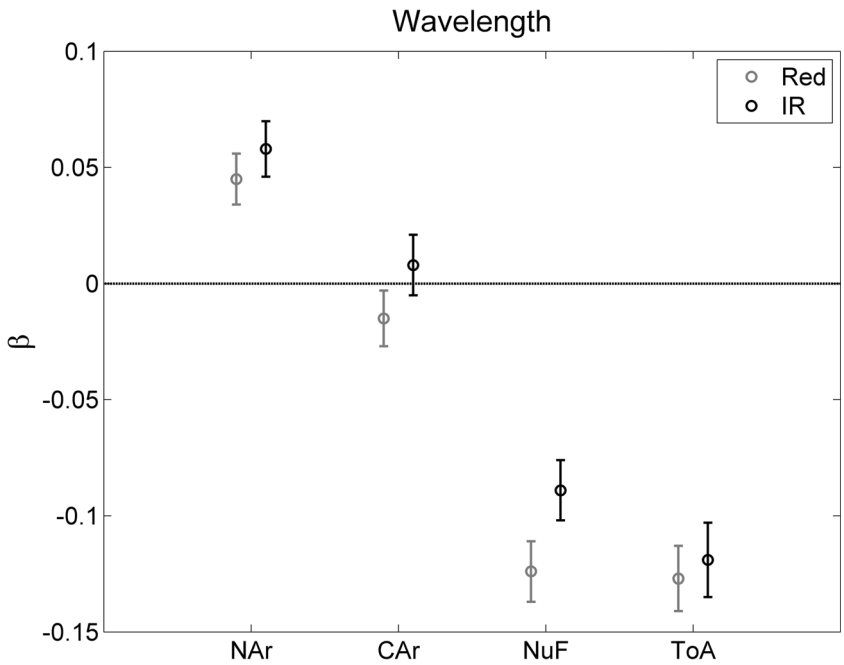

Fig. 3 Coefficients β for the analysed variables as a function of photobiomodulation wavelength. The analysed variables are nuclear area *NAr*, cell area *CAr*, number of filaments *NuF*, and total actin *ToA*. The error bars indicate the standard error of the mean (SEM)

Table 4 Values of the β coefficients for the separation of the wavelength. Two asterisk symbols indicate that the coefficients are different from zero, according to the Z test and $p < 0.01$. There is no significant difference between the coefficients, when comparing the red and IR wavelengths, according to Z test and $p < 0.05$. The number in parentheses is the uncertainty of the coefficient in the last(s) decimal(s). The analysed variables are nuclear area *NAr*, cell area *CAr*, number of filaments *NuF* and total actin *ToA*

Coefficients	*NAr*	*CAr*	*NuF*	*ToA*
β_{Red}	+ 0.045 (11)**	− 0.015 (12)	− 0.124 (13)**	− 0.127 (14)**
β_{IR}	+ 0.058 (12)**	+ 0.008 (13)	− 0.089 (13)**	− 0.119 (16)**

different from zero, for the *NAr*, *ToA*, and *NuF*. In addition, for the *CAr*, both coefficients are compatible with zero. This means that the PBM treatment–induced changes are equally efficient at both wavelengths. While one of the main wavelength influences in vivo is the photon's penetration in the biological tissue, it does not affect in vitro experiments. However, considering the PBM-induced photophysical and photochemical effects are quantum processes, the difference in the photon quantum energy of 1.983 eV versus 1.535 eV must be considered. Thus, considering the radiant exposures, the photon density for 808 nm was 30 to 35% higher to achieve similar results.

Analysing the data as a function of growth substrate stiffness is shown in Fig. 4 and Table 5. The coefficients are significantly different from zero, except for the *CAr*. However, no significant differences were observed between the β coefficients when comparing the 4 kPa and the 16 kPa gels.

The results for the separation of data according to incubation time post-PBM treatment are shown in Fig. 5 and Table 6. For the *NAr*, *NuF*, and *ToA*, the β coefficient for 24 h is closer to zero than the same coefficients for 5 min and 1 h post-PBM. These findings suggest that the PBM treatment effect in the cells might be short term on a time scale of hours. This estimate is supported by the fact that the 24-h β coefficient for the *NAr* is not different from zero.

Simultaneous influence of all parameters

From the individual analysis of each experimental parameter, there is evidence that the time post-PBM treatment is the dominant confounder for the observed results. Conversely, there is evidence that the PBM wavelength and the gel stiffness are only responsible for minor corrections. Because of that, we assumed that the β coefficient could be described as in Eq. 4. In this equation, β_{time} is the main component, referent to the time post-PBM treatment, which has three possibilities: β_{5min}, β_{1h}, or β_{24h}. For the wavelength and gel stiffness, the corresponding δ coefficient could check for the minor corrections related to these parameters. Thus, for the red light, a positive coefficient ($+\delta_{wavelength}$) was put in the equation while for the NIR light, a negative coefficient ($-\delta_{wavelength}$) was used. The same procedure was executed for the gel stiffness, for the 4 kPa ($+\delta_{gel}$) and the 16 kPa ($-\delta_{gel}$) gels. Hence, a δ coefficient different from zero indicates that there is an effect related to the parameter of that coefficient. Hence, if the respective δ are different

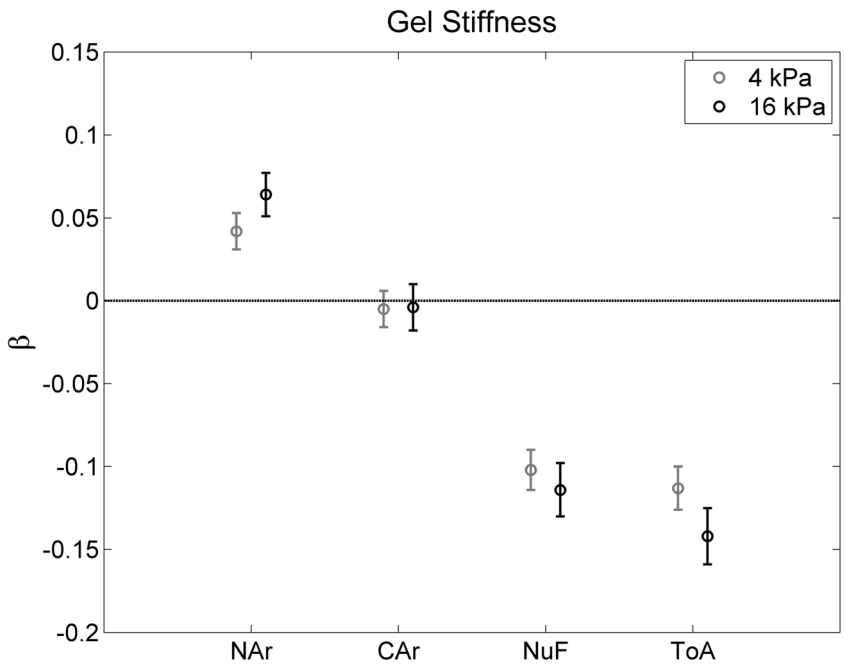

Fig. 4 β coefficients for the analysed variables, with the gel stiffness separation. The analysed variables are nuclear area *NAr*, cell area *CAr*, number of filaments *NuF*, and total actin *ToA*. The error bars indicate the standard error of the mean (SEM)

Table 5 Values of the β coefficients as a function of the gel stiffness. Two asterisk symbols indicate that the coefficients are different from zero, according to the Z test and $p < 0.01$. There is no significant difference between the coefficients, when comparing the 4 kPa and the 16 kPa gels, according to Z test and $p < 0.05$. The number in parentheses is the uncertainty of the coefficient in the last(s) decimal(s). The analysed variables are nuclear area *NAr*, cell area *CAr*, number of filaments *NuF*, and total actin *ToA*

Coefficients	*NAr*	*CAr*	*NuF*	*ToA*
β_{4kPa}	+ 0.042 (11)**	− 0.005 (11)	− 0.102 (12)**	− 0.113 (13)**
β_{16kPa}	+ 0.064 (13)**	− 0.004 (14)	− 0.114 (16)**	− 0.142 (17)**

from zero, the respective parameters are not equivalent, with its absolute value indicating the strength of the effect, and the signs indicating the conditions driving the effect on the cytoskeleton. However, if the δ is not different from zero, the corresponding confounder has no effect on the efficacy of the PBM treatment.

$$\beta = \beta_{time} + \delta_{wavelength} + \delta_{gel} \quad (4)$$

Table 7 shows β_{time}, $\delta_{wavelength}$, and δ_{gel} coefficients when all experimental parameters are taken into account. The influence of the wavelength and gel stiffness is the same as when those parameters were analysed individually: no difference was identified between the red and NIR wavelengths and between the two gel stiffness used. On the other hand, the time post-PBM treatment has a large influence on the results, which are similar to those obtained when analysing time individually. Furthermore, the compatibilities between the coefficients of the different incubation times after PBM treatment are the same.

At last, an alternative graphic analysis of the PBM treatment effect was performed. The same differences presented so far can also be qualitatively verified, with graphs of the relationship between pairs of variables, regardless of the cell number. The full description of this analysis and the results are presented in the Appendix (Alternative graphic analysis of the PBM treatment effect subsection), in Fig. 8.

Discussion

Actin filaments are continuously changing, and their remodelling is very rapid and hence, the observation of differences in the actin filaments, 5 min after PBMT, is reasonable, due to this quick response. Ballestrem and colleagues investigated the dynamics of actin filaments in migratory cells. They imaged cells at intervals of 3 min and detected differences in the actin filaments between images [25]. Furthermore, studies

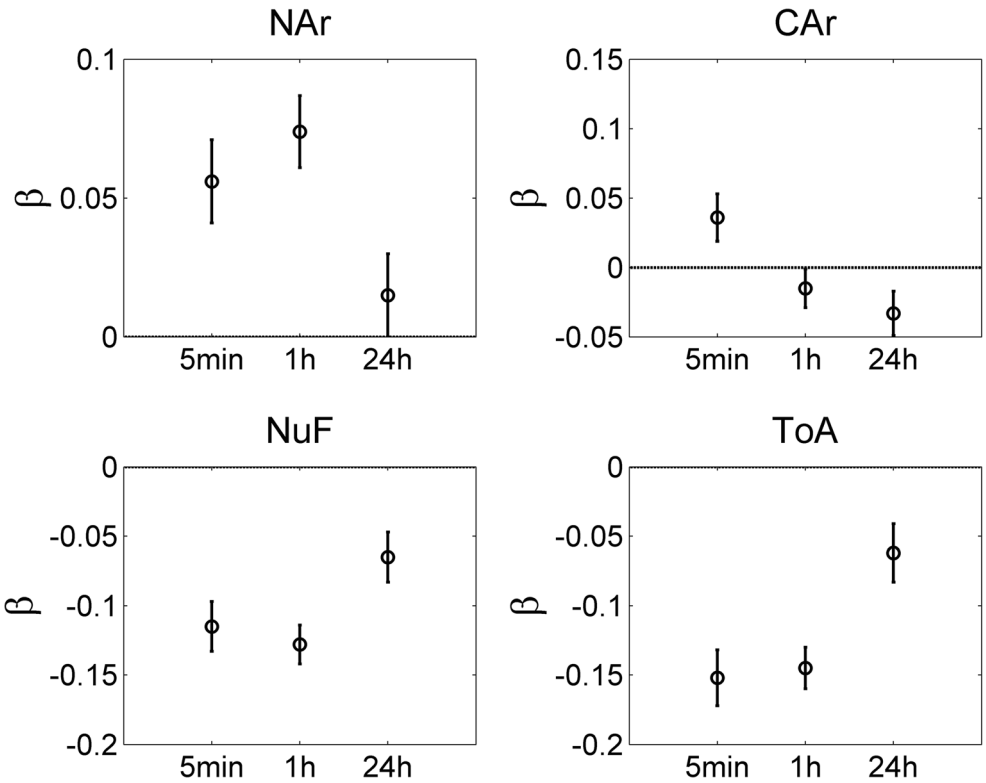

Fig. 5 β coefficients for the analysed variables, as a function of time post-photobiomodulation treatment. The analysed variables are nuclear area *NAr*, cell area *CAr*, number of filaments *NuF*, and total actin *ToA*. The error bars indicate the standard error of the mean (SEM)

Table 6 Values of the β coefficients for the data separation according to the incubation time post-PBM treatment. One asterisk symbol indicates that the coefficients are different from zero, according to the Z test and $p < 0.05$, and two asterisks indicate $p < 0.01$. The compatibilities between the pairs of times are indicated by the symbols \$ (5 min and 24 h) and & (1 h and 24 h), for the Z test and $p < 0.01$. No differences were found between the 5 min and 1 h coefficients. The number in parentheses is the uncertainty of the coefficient in the last(s) decimal(s). The analysed variables are nuclear area *NAr*, cell area *CAr*, number of filaments *NuF*, and total actin *ToA*

Coefficients	*NAr* (&)	*CAr* (\$)	*NuF* (&)	*ToA* (\$&)
β_{5min}	+ 0.056 (15)**	+ 0.036 (17)*	− 0.115 (18)**	− 0.152 (20)**
β_{1h}	+ 0.074 (13)**	− 0.015 (14)	− 0.128 (14)**	− 0.145 (15)**
β_{24h}	+ 0.015 (15)	− 0.033 (16)*	− 0.065 (18)**	− 0.062 (21)**

with cytochalasins (a substance known due to its effects on actin filaments) show that the drug effect in the cells starts in minutes [25, 26]. This means that the actin filaments are very responsive to the action of external stimuli, as potentially the PBM treatment used in this work.

For the *CAr*, the 5-min and 24-h β coefficients are incompatible with zero with $p < 0.05$ and show opposite effects: an increase in the *CAr* of 3.5% at 5 min and a decrease of 3.8% at 24 h. However, for the *CAr*, in both cases, the p values are in the range of $0.01 < p < 0.05$ (for all other incompatible cases, the p values are smaller than 0.0002). Therefore, the results for the *CAr* might not be as reliable as the other parameters, as the observed difference might have occurred by chance. Indeed, as about 80 statistical tests were made in this work, it is possible to have few cases of $p < 0.05$ just by chance. An interesting result found is that the magnitude of the effect caused in the *NuF* and in the *ToA* is very similar. This agrees with the expectation that those variables access the same type of information; so, they are two ways of measuring the variation due to the PBM treatment in the actin filaments.

The number of variables used in this work is large, as we intended to observe modifications in the cytoskeleton. An issue that arises when the separation of the parameters is performed is the decrease in the amount of data used to determine each parameter, as the number of images in each group is reduced impacting the power of the statistical analysis.

One limitation of the study pertains to the pairing of experimental conditions, which means to pair samples with a particular set of confounders to a control group with the same set of confounders. Ideally, all parameters should have been changed at the same time as other, non-controlled variables, would influence the results less. Unfortunately, the magnitude of the required sample size precluded this.

A study using optical tweezers to photo-stimulate 3T3 cells showed that morphological changes appear in 28% of the cells post-stimulation, in contrast with 18% of cells showing morphological changes in the control samples [15]. This is consistent with our findings that the differences are not obvious if the confocal images are analysed only visually. However, if analysed objectively, small but distinct differences are observed between samples globally. Our analysis showed that there is a slight increase, around 5%, in the *NAr*, and a decrease of around 12% in the *NuF* and the *ToA*.

It is worth to stress that further studies are necessary to evaluate if the cell changes due to PBM reported in this work lead to effective biological modifications and whether or not these cell changes are related with the PBMT mechanism of action.

Conclusion

In conclusion, this experiment indicated that photobiomodulation therapy could change the morphological properties of cells and their cytoskeleton. In particular, the PBM treatment causes a reduction in the number of actin filaments and the amount of polymerized actin, in the cells. Furthermore, the PBM treatment also slightly increases the nuclear area, without significant modifications in the cell area. All the cited effects diminish or disappear if the cells are incubated for periods of several hours after the

Table 7 Values of the β_{time}, $\delta_{wavelength}$, and δ_{gel} coefficients for the separation for all experimental parameters at the same time. One asterisk symbol indicates that the coefficients are different from zero, according to the Z test and $p < 0.05$, and two asterisks indicate $p < 0.01$. The compatibilities between the pairs of times are indicated by the symbols \$ (5 min and 24 h) and & (1 h and 24 h), for the Z test and $p < 0.01$. No differences were found between the 5 min and 1 h coefficients. The number in parentheses is the uncertainty of the coefficient in the last(s) decimal(s). The analysed variables are nuclear area *NAr*, cell area *CAr*, number of filaments *NuF*, and total actin *ToA*

Coefficients	*NAr* (&)	*CAr* (\$)	*NuF* (&)	*ToA* (\$&)
β_{5min}	+ 0.057 (15)**	+ 0.035 (17)*	− 0.122 (19)**	− 0.158 (20)**
β_{1h}	+ 0.079 (14)**	− 0.013 (14)	− 0.130 (15)**	− 0.151 (16)**
β_{24h}	+ 0.016 (15)	− 0.033 (16)*	− 0.070 (18)**	− 0.065 (21)**
$\delta_{wavelength}$	+ 0.006 (8)	+ 0.011 (9)	+ 0.016 (10)	+ 0.004 (11)
δ_{gel}	+ 0.012 (9)	0.000 (9)	− 0.013 (10)	− 0.019 (11)

PBM treatment. This indicates that PBM treatment, as an external stimulus, causes transient structural modifications. This is an important result because despite the light radiation being an external source of stress to the cells, the damage caused is not permanent. Although our analysis reveals these cell modifications due to PBM, the relevance of the biological effects related to them still need to be evaluated. Also, the implications of the modifications to the functionality of the cells should be checked. Further investigations are required to determine the specific mechanisms involved and how this phenomenon is related to the PBMT mechanisms of action.

Funding This study was funded by Coordination for the Improvement of Higher Education Personnel, CAPES (Proc. No. BEX 3481/14-0), and Brazilian National Council for Scientific and Technological Development, CNPq, Brazilian funding agencies. Additional support was provided by the Ontario Ministry of Health and Long-Term Care through operational funding of the Princess Margaret Cancer Centre.

Compliance with ethical standards

Conflict of interest The authors declare that they have no conflict of interest.

Ethical approval This article does not contain any studies with human participants or animals performed by any of the authors.

Appendix. Data analysis details

Raw data analysis

With the primary data extracted from the images, several quantitative studies were performed. At first, the number of cells in each image was determined, resulting in the histograms shown in Fig. 6 for the control and PBM-treated groups. The majority of images has between three and nine cells; however, there were some images with more than 13 cells.

As the distributions of the cell density per image are similar, subsequent investigations considered only the different number of cells per image, and the four variables, *CAr* (cell area), *NAr* (nuclear area), *NuF* (number of filaments), and *ToA* (total actin), for further analysis. For the control group, the four parameters are shown as a function of cells per image in Fig. 7. The dependencies are approximately linear with cell number. However, a small deviation from the linearity is observed for all the investigated variables in the case of a high cell density. The same behaviour is also noted in the PBM group.

A linear function $Y(N) = a\,N$ (where Y is the analysed variable—*NAr*, *CAr*, *NuF*, or *ToA*; N is the number of cells in the image; and a is the slope) would be adequate only for images with low cell densities. However, in order to adjust for the deviation from linearity at high cell densities, a fit required a small quadratic term as shown in Eq. A.1, where γ was determined from the global relation between Y and N for all data. The resulting γ coefficients are small: 0.0095, 0.0180, 0.0088, and 0.0057, for *NAr*, *CAr*, *NuF*, and *ToA*, respectively.

$$Y(N) = a\,N\,(1-\gamma N) \tag{A.1}$$

The uncertainty, σ_N, for each $Y(N)$ variable (*NAr*, *CAr*, *NuF*, or *ToA*) was determined as a function of the image's cell density. Considering the statistical variation in Y due to each cell as σ_1, in an image with N cells, the uncertainty of $Y(N)$ can be estimated by standard uncertainty propagation, leading to $\sigma_N = \sigma_1\sqrt{N}$, where σ_N is the uncertainty for that number of cells. In the fittings, the uncertainty in each variable for each cell, σ_1, was found from the overall variance of the data around the fitted functions, assuming the hypothesis that the χ^2 is equal to the degrees of freedom, or that $\chi^2_R = 1$. This allows to estimate σ_1 and the uncertainty of the fitted parameters with a large number of degrees of freedom (~ 1660).

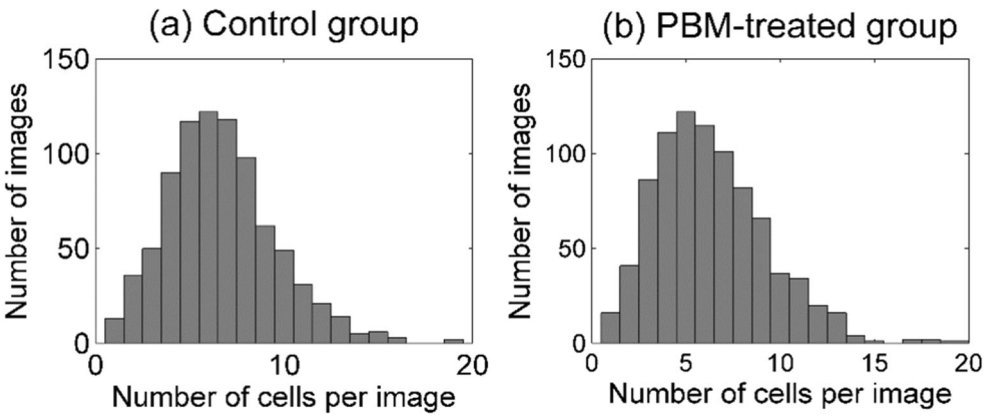

Fig. 6 Histogram of the number of cells per image, for the control group (**a**) and photobiomodulation-treated group (**b**). Less than 10% of images have more than ten cells, for both groups

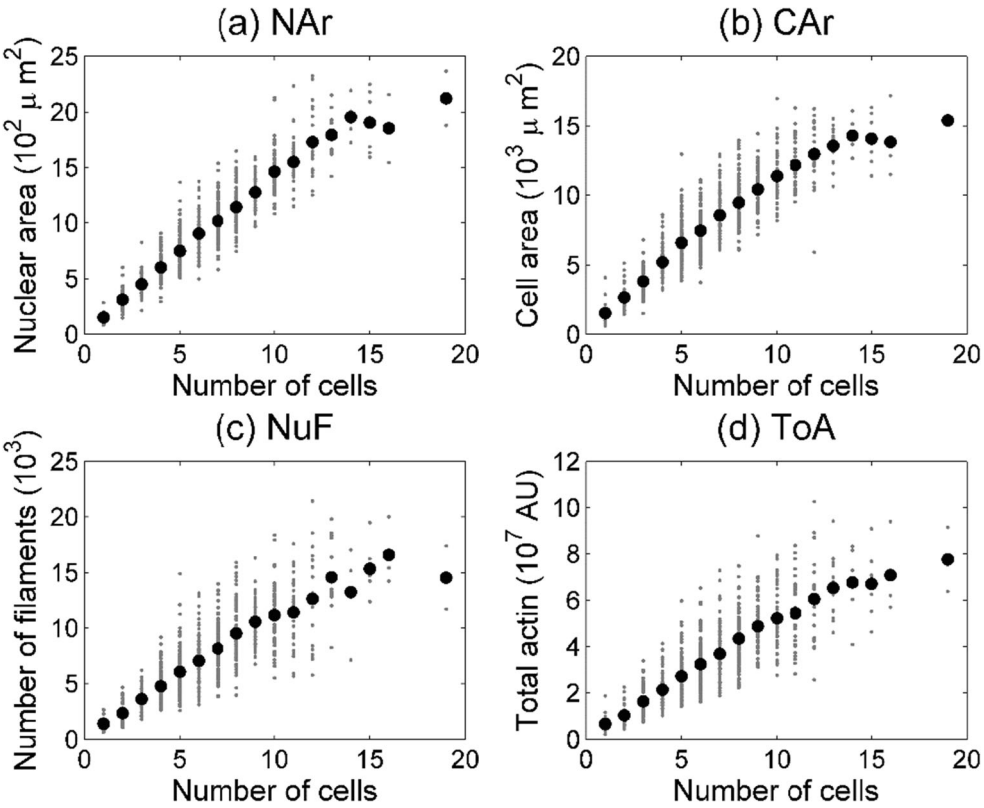

Fig. 7 Raw data for all variables, nuclear area *NAr* (**a**), cell area *CAr* (**b**), number of filaments *NuF* (**c**), and total actin *ToA* (**d**), for the control group. The large symbols represent the average for each number of cells. The behaviour of each of the variables with the number of cells is approximately linear. However, a small deviation from the linearity is perceived at high cell densities. The 837 images of the control groups (non-photobiomodulation) contributed to these data

Table 8 Results of the *p* values for the *Z* test, for the comparison of β with zero, for the global analysis

Coefficient	*NAr*	*CAr*	*NuF*	*ToA*
β	$<10^{-9}$**	0.60	$<10^{-16}$**	$<10^{-16}$**

Table 9 Results of the *p* values for the *Z* test, for the comparison of β with zero, as a function of the wavelength

Coefficients	*NAr*	*CAr*	*NuF*	*ToA*
β_{red}	$<10^{-4}$**	0.20	$<10^{-16}$**	$<10^{-16}$**
β_{IR}	$<10^{-5}$**	0.56	$<10^{-10}$**	$<10^{-13}$**

Table 10 Results of the *p* values for the *Z* test, for the comparison of the β coefficients between them, as a function of the wavelength

Compared pair	*NAr*	*CAr*	*NuF*	*ToA*
β_{red}/β_{IR}	0.41	0.20	0.64	0.70

Table 11 Results of the *p* values for the *Z* test, for the comparison of β with zero, as a function of the gel stiffness

Coefficients	*NAr*	*CAr*	*NuF*	*ToA*
β_{4kPa}	$<10^{-4}$**	0.64	$<10^{-16}$**	$<10^{-16}$**
β_{16kPa}	$<10^{-5}$**	0.80	$<10^{-12}$**	$<10^{-15}$**

Table 12 Results of the *p* values for the *Z* test, for the comparison of the β coefficients between them, as a function of the gel stiffness

Compared pair	*NAr*	*CAr*	*NuF*	*ToA*
$\beta_{4kPa}/\beta_{16kPa}$	0.20	0.92	0.56	0.18

Table 13 Results of the *p* values for the *Z* test, for the comparison of β with zero, as a function of the time post-PBM treatment

Coefficients	*NAr*	*CAr*	*NuF*	*ToA*
β_{5min}	0.0002**	0.033*	$<10^{-9}$**	$<10^{-13}$**
β_{1h}	$<10^{-7}$**	0.28	$<10^{-16}$**	$<10^{-16}$**
β_{24h}	0.33	0.047*	0.0003**	0.003**

Table 14 Results of the p values of the Z test, for the comparison of the β coefficients between them, as a function of the time post-PBM treatment

Compared pairs	*NAr*	*CAr*	*NuF*	*ToA*
β_{5min}/β_{1h}	0.37	0.019*	0.56	0.78
β_{5min}/β_{24h}	0.051	0.004**	0.052	0.002**
β_{1h}/β_{24h}	0.003**	0.41	0.005**	0.001**

Table 15 Results of the p values for the Z test, for the comparison of β with zero, for the simultaneous influence of all parameters

Coefficients	*NAr*	*CAr*	*NuF*	*ToA*
β_{5min}	0.0001**	0.035*	$<10^{-10}$**	$<10^{-14}$**
β_{1h}	$<10^{-8}$**	0.37	$<10^{-16}$**	$<10^{-16}$**
β_{24h}	0.29	0.044*	0.0001**	0.002**
$\delta_{wavelength}$	0.45	0.23	0.11	0.71
δ_{gel}	0.17	0.96	0.20	0.086

Table 16 Results of the p values of the Z test, for the comparison of β of each time post-PBM treatment, between them, for the simultaneous influence of all parameters

Compared pairs	*NAr*	*CAr*	*NuF*	*ToA*
β_{5min}/β_{1h}	0.29	0.029*	0.75	0.80
β_{5min}/β_{24h}	0.049*	0.004**	0.045*	0.001**
β_{1h}/β_{24h}	0.002**	0.35	0.010**	0.001**

p values of the statistical tests

For Tables 8, 9, 11, 13, and 15, one asterisk symbol indicates that the coefficients are different from zero, according to the Z test and $p < 0.05$, and two asterisks indicate $p < 0.01$. For Tables 10, 12, 14, and 16, one asterisk symbol indicates that the coefficients are different from each other, according to the Z test and $p < 0.05$, and two asterisks indicate $p < 0.01$.

Alternative graphic analysis of the PBM treatment effect

The same differences presented in the paper can also be qualitatively verified, with graphs of the relationship between pairs of variables, regardless of the cell number, as shown in the scatter plots of Fig. 8. Indeed, the highest difference between the control and PBM-treated groups appears when the variables plotted have variations in opposite directions, which means β positive for one variable and negative for the other. Figure 8a shows an example of this case with the number of filaments as a function of the nuclear area indicating that the PBM treatment leads to a reduction in the number of filaments in images with a similar nuclear area. On the other hand, if the plotted variables have variations in the same direction (β with the same signal), it is not possible to see differences between control and treated groups, as shown in Fig. 8b, for the total actin and number of filaments. This analysis method has the advantage to be insensitive to the hypotheses expressed in Eq. A.1. While this alternative method is unable to explain the cause of the differences or lack thereof, it is an indication of the former analysis' robustness.

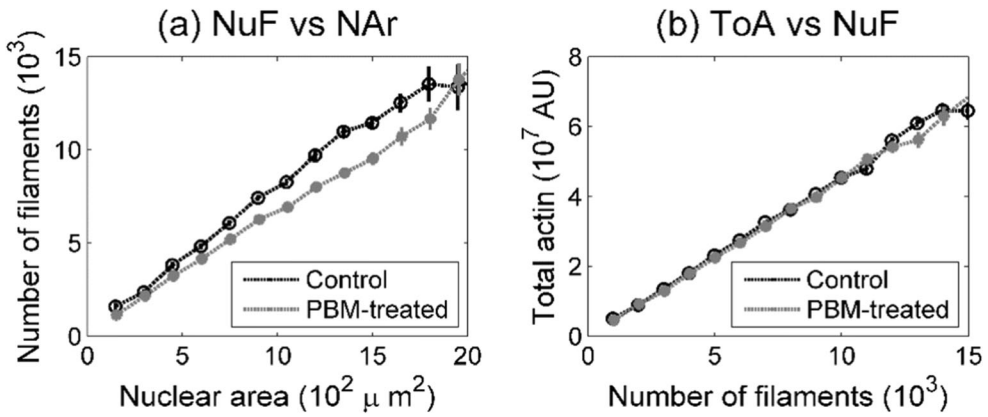

Fig. 8 Examples of graphs of the relationship between pairs of variables, black symbols represent the control samples and grey symbols the photobiomodulation-treated samples. Number of filaments *NuF* versus nuclear area *NAr* (a) is a case that has the β coefficients with different signals (*NAr* has a positive β and the *NuF* has a negative β), and total actin versus number of filaments (b) is a case that the β coefficients have the same signal for both the *ToA* and *NuF* (both have negative β coefficents). The lines connecting the points are a visual guide only. The error bars indicate the standard error of the mean (SEM)

References

1. Chung H, Dai T, Sharma SK, Huang Y-Y, Carroll JD, Hamblin MR (2012) The nuts and bolts of low-level laser (light) therapy. Ann Biomed Eng 40:516–533. https://doi.org/10.1007/s10439-011-0454-7
2. Tata DB, Waynant RW (2011) Laser therapy: a review of its mechanism of action and potential medical applications. Laser Photon Rev 5:1–12. https://doi.org/10.1002/lpor.200900032
3. Karu T (1999) Primary and secondary mechanisms of action of visible to near-IR radiation on cells. J Photochem Photobiol B 49: 1–17. https://doi.org/10.1016/S1011-1344(98)00219-X
4. Amat A, Rigau J, Waynant RW, Ilev IK, Anders J (2006) The electric field induced by light can explain cellular responses to electromagnetic energy: a hypothesis of mechanism. J Photochem Photobiol B Biol 82:152–160
5. Karu TI, Pyatibrat LV, Afanasyeva NI (2004) A novel mitochondrial signaling pathway activated by visible-to-near infrared radiation. Photochem Photobiol 80:366–372. https://doi.org/10.1562/2004-03-25-RA-123
6. Chang HY, Chi J-T, Dudoit S, Bondre C, van de RM, Botstein D, Brown PO (2002) Diversity, topographic differentiation, and positional memory in human fibroblasts. Proc Natl Acad Sci 99:12877–12882. https://doi.org/10.1073/pnas.162488599
7. Rieske P, Krynska B, Azizi SA (2005) Human fibroblast-derived cell lines have characteristics of embryonic stem cells and cells of neuro-ectodermal origin. Differentiation 73:474–483. https://doi.org/10.1111/j.1432-0436.2005.00050.x
8. Peplow PV, Chung T-Y, Baxter GD (2010) Laser photobiomodulation of proliferation of cells in culture: a review of human and animal studies. Photomed Laser Surg 28:S–3-S-40. https://doi.org/10.1089/pho.2010.2771
9. Ragoonanan V, Less R, Aksan A (2013) Response of the cell membrane-cytoskeleton complex to osmotic and freeze/thaw stresses. Part 2: the link between the state of the membrane-cytoskeleton complex and the cellular damage. Cryobiology 66: 96–104. https://doi.org/10.1016/j.cryobiol.2012.10.008
10. Liu L, Luo Q, Sun J, Song G (2016) Nucleus and nucleus-cytoskeleton connections in 3D cell migration. Exp Cell Res 348: 56–65. https://doi.org/10.1016/j.yexcr.2016.09.001
11. Toh KC, Ramdas NM, Shivashankar GV (2015) Actin cytoskeleton differentially alters the dynamics of lamin A, HP1α and H2B core histone proteins to remodel chromatin condensation state in living cells. Integr Biol 7:1309–1317. https://doi.org/10.1039/C5IB00027K
12. Chow RT, David MA, Armati PJ (2007) 830 nm laser irradiation induces varicosity formation, reduces mitochondrial membrane potential and blocks fast axonal flow in small and medium diameter rat dorsal root ganglion neurons: implications for the analgesic effects of 830 nm laser. J Peripher Nerv Syst 12:28–39. https://doi.org/10.1111/j.1529-8027.2007.00114.x
13. Ricci R, Pazos MC, Borges RE, Pacheco-Soares C (2009) Biomodulation with low-level laser radiation induces changes in endothelial cell actin filaments and cytoskeletal organization. J Photochem Photobiol B 95:6–8. https://doi.org/10.1016/j.jphotobiol.2008.11.007
14. Houreld NN, Ayuk SM, Abrahamse H (2014) Expression of genes in normal fibroblast cells (WS1) in response to irradiation at 660nm. J Photochem Photobiol B 130:146–152. https://doi.org/10.1016/j.jphotobiol.2013.11.018
15. Avila R, Medina-Villalobos N, Tamariz E, Chiu R, Lopez-Marín LM, Acosta A, Castaño V (2014) Optical tweezers experiments for fibroblast cell growth stimulation. Proccedings SPIE 9129:91291U. https://doi.org/10.1117/12.2064939
16. Sassoli C, Chellini F, Squecco R, Tani A, Idrizaj E, Nosi D, Giannelli M, Zecchi-Orlandini S (2016) Low intensity 635 nm diode laser irradiation inhibits fibroblast-myofibroblast transition reducing TRPC1 channel expression/activity: new perspectives for tissue fibrosis treatment. Lasers Surg Med 48:318–332. https://doi.org/10.1002/lsm.22441
17. Fischer RS, Myers KA, Gardel ML, Waterman CM (2012) Stiffness-controlled three-dimensional extracellular matrices for high-resolution imaging of cell behavior. Nat Protoc 7:2056–2066. https://doi.org/10.1038/nprot.2012.127
18. Niu CJ, Fisher C, Scheffler K, Wan R, Maleki H, Liu H, Sun Y, Simmons C A, Birngruber R, Lilge L (2015) Polyacrylamide gel substrates that simulate the mechanical stiffness of normal and malignant neuronal tissues increase protoporphyin IX synthesis in glioma cells. J Biomed Opt 20:098002-1–7. https://doi.org/10.1117/1.JBO.20.9.098002
19. Rotsch C, Jacobson K, Radmacher M (1999) Dimensional and mechanical dynamics of active and stable edges in motile fibroblasts investigated by using atomic force microscopy. PNAS Cell Biol 96:921–926
20. Schindelin J, Arganda-Carreras I, Frise E, Kaynig V, Longair M, Pietzsch T, Preibisch S, Rueden C, Saalfeld S, Schmid B, Tinevez J-Y, White DJ, Hartenstein V, Eliceiri K, Tomancak P, Cardona A (2012) Fiji: an open-source platform for biological-image analysis. Nat Methods 9:676–682. https://doi.org/10.1038/nmeth.2019
21. The MathWorks I (2013) MATLAB and Statistics Toolbox Release 2013b
22. Kreutzer J, Viehrig M, Maki AJ, Kallio P, Rahikainen R, Hytönen V (2017) Pneumatically actuated elastomeric device for simultaneous mechanobiological studies & live-cell fluorescent microscopy. Int Conf Manip Autom Robot Small Scales, MARSS 2017 - Proc. https://doi.org/10.1109/MARSS.2017.8001929
23. Lee TC, Kashyap RL, Chu CN (1994) Building skeleton models via 3-D medial surface axis thinning algorithms. CVGIP Graph Model Image Process 56:462–478. https://doi.org/10.1006/cgip.1994.1042
24. Arganda-Carreras I, Fernández-González R, Muñoz-Barrutia A, Ortiz-De-Solorzano C (2010) 3D reconstruction of histological sections: application to mammary gland tissue. Microsc Res Tech 73: 1019–1029. https://doi.org/10.1002/jemt.20829
25. Ballestrem C, Wehrle-Haller B, Imhof BA (1998) Actin dynamics in living mammalian cells. J Cell Sci 111:1649–1658
26. Rotsch C, Radmacher M (2000) Drug-induced changes of cytoskeletal structure and mechanics in fibroblasts: an atomic force microscopy study. Biophys J 78:520–535. https://doi.org/10.1016/S0006-3495(00)76614-8